High-birefringence, low-loss porous fiber for single-mode terahertz-wave guidance

Article *in* Applied Optics · July 2013
DOI: 10.1364/AO.52.005297 · Source: PubMed

3 authors, including:

Jian Liang
Xi'an Institute of Optics and Fine Mechanics
72 PUBLICATIONS **369** CITATIONS
SEE PROFILE

Liyong Ren
Xi'an Institute of Optics and Fine Mechanics
128 PUBLICATIONS **909** CITATIONS
SEE PROFILE

High-birefringence, low-loss porous fiber for single-mode terahertz-wave guidance

Na-na Chen,[1,2] Jian Liang,[1,2] and Li-yong Ren[1,*]

[1]State Key Laboratory of Transient Optics and Photonics, Xi'an Institute of Optics and Precision Mechanics, Chinese Academy of Sciences, Xi'an 710119, China

[2]University of Chinese Academy of Sciences, Beijing 100049, China

*Corresponding author: renliy@opt.ac.cn

Received 28 May 2013; revised 27 June 2013; accepted 28 June 2013; posted 1 July 2013 (Doc. ID 191353); published 19 July 2013

A new kind of polymer porous fiber with elliptical air-holes is designed for obtaining high birefringence in the terahertz (THz) frequency range in this paper. Using the finite element method, the properties of this kind of fiber are simulated in detail including the single-mode propagation condition, the birefringence, and the loss. Theoretical results indicate that the single-mode THz wave in the frequency range from 0.73 to 1.22 THz can be guided in the fiber; the birefringence can be enhanced by rotating the major axis of the elliptical air-hole and there exists an optimal rotating angle at 30°. At this optimal angle a birefringence as high as 0.0445 can be obtained in a wide frequency range. Low-loss THz guidance can be achieved owing to the effective reduction of the material absorption in such a porous fiber. This research is useful for polarization-maintaining THz-wave guidance.

OCIS codes: (040.2235) Far infrared or terahertz; (060.2420) Fibers, polarization-maintaining; (060.4005) Microstructured fibers; (160.5470) Polymers.

http://dx.doi.org/10.1364/AO.52.005297

1. Introduction

In past decades, a special and narrow segment [covering the frequency range of 0.1–10 THz (1 THz = 10^{12} Hz)] of the whole electromagnetic-spectrum family, so-called terahertz (THz), has been a durative hot topic due to its increasing number of promising and potential application fields. These include sensing [1], imaging [2], biotechnology [3], security [4], astronomy [5], spectroscopy [6], etc. Generally speaking, THz technology involves three major parts: the THz source, the THz waveguide, and the THz detector. Among them, the THz source has been generally commercial, and the THz detector such as the spectrum and/or imaging facilities have also been put on the market. Relatively, the waveguide available for effectively transmitting THz waves is not enough so far. Therefore, the research of the low-loss THz waveguide for finely connecting the other two parts becomes indispensable.

However, there exists great challenges in the study of THz transmission. On one hand, almost all of the materials show high absorption coefficients in the THz frequency range except dry air. On the other hand, in most of the THz systems the THz beam is usually coupled, transported, and/or managed in free space, which requires precision alignment and maintenance. Thus, uncertain loss influenced by the surroundings would be inevitably brought in. To overcome these obstacles, lots of effort has been put into developing various forms of THz waveguides. For instance, metal wires [7,8] and metal coating medium tube waveguides [9,10] were proposed in the early stages. However, metal waveguides usually have the disadvantages of high bending loss, low coupling efficiency, and unstable guidance in complex surroundings [11,12]. Recently, hotspot have been turning toward polymer fibers, such as Bragg band-gap fibers [13], plastic photonic bandgap fibers [14–16], subwavelength porous fibers

1559-128X/13/215297-06$15.00/0

[11,12,17–19], hollow core fibers [20] and so on. Among them, the subwavelength porous fibers have been proven to exhibit some merits, such as extremely low loss, flexibleness in fabrication, and small fiber diameter [11,12,17,19].

Besides the low-loss property, highly birefringent porous THz fibers demonstrate a positive function in polarization maintaining, which exhibits many potential applications in polarized THz filters and sensors. It is known from traditional photonic crystal fibers (PCFs) that high birefringence can be achieved by mainly using two methods. One method is to introduce the asymmetry to the fiber core [21,22]; the other is to break the symmetry of the fiber cladding [23]. Unlike the structure of PCFs, the core of the porous fiber is full of holes which are much larger in size, and the cladding is the air background. Therefore, one can realize the high birefringence in the porous core by modifying the geometric parameters of the air holes in the core.

For the first time, Atakaramians *et al.* [24,25] designed and fabricated a rectangular porous fiber with high birefringence of 0.012 at $f = 0.65$ THz. Later, Chen *et al.* [18] proposed a squeezed lattice elliptical-hole THz fiber with high birefringence, whose results show that with a moderate amount of deformation, the fiber exhibits high birefringence on a level of 10^{-2}. However, this kind of porous fiber is hard to fabricate; besides, the elliptical-shape head face inevitably increases the difficulty in coupling, which makes it inconvenient for practical applications. Trying to settle these problems and maintaining the high birefringence simultaneously, we present a design of porous THz fiber containing a hexagonal array of subwavelength elliptical holes. And by rotating the major axis' direction of the elliptical hole, we find that the birefringence can be enhanced. Numerical simulations indicate that there exists an optimal rotation angle at 30° and at this angle the fiber usually possesses good properties of high birefringence and low loss. What's worth mentioning is that, for all the simulations presented in this paper, the parameters of the porous fiber are chosen to ensure the THz wave can only be guided in the fundamental-mode fashion. Please note that this point is very important and is usually neglected by many other researchers.

2. Model Design

We choose Topas cyclic-olefin copolymer (COC) as the fiber material. This choice is based on the following considerations: (1) owing to the amorphous structure of the nonpolar COC, the bulk material loss of it is approximately 100 times lower than that of polymethylmethacrylate (PMMA); (2) the refractive index of it is nearly a constant of 1.5258 in the frequency range of 0.1–1.5 THz [26], which is beneficial for ultra-low material dispersion; (3) it hardly absorbs water vapor, which is an absolute advantage in making THz waveguides. The schematic diagram of the porous fiber we proposed is indicated in Fig. 1. The air holes are arranged in the triangular lattices. Λ is the pitch between the center to center lattice and ρ is the ellipticity of the air hole defined by the length ratio of the minor axis to the major one. In all the simulations of this paper, we choose Λ as 40 μm, the major axis (2b) and the minor axis (2a) as 36 and 21.6 μm, respectively, thus leading $\rho = 0.6$. These parameters ensure that the guided mode works at the frequency around 1 THz.

The single mode condition is determined by the normalized frequency (i.e., V-parameter) expressed by

$$V = \frac{2\pi r f}{c}\sqrt{n_{\mathrm{co}}^2 - n_{\mathrm{cl}}^2} \le 2.405, \tag{1}$$

where r is the radius of the fiber core, f is the frequency, c is the speed of light in vacuum, and n_{co} and n_{cl} are the effective indices of the fiber core and cladding, respectively. Since the cladding for this microstructure fiber is air background, n_{cl} can be regarded as 1. Besides, we regard n_{co} to be n_{eff} due to the porous structure in the core region. It's easy to find that parameters which might affect the value of V are the r, f and n_{eff}. Take the operating frequency at 1 THz as an example, r and n_{eff} of the fiber in the single mode propagation condition are limited by the relation of $r\sqrt{n_{\mathrm{eff}}^2 - 1} < 114.89$ (here the unit of r is μm). Considering the fact that n_{eff} increases as r, there exists a restriction in the value of r for keeping the single mode guidance. In our simulations, $r = 3.5\Lambda$ is selected to guarantee the fiber working only under the fundamental mode. In this case, the fiber core contains 3 rings of air holes.

It is easy to know from Eq. (1) and the physical meaning of n_{eff} that this kind of porous fiber can keep just the single-mode working status within a specific frequency region determined by the geometrical parameters of the fiber. In what follows, we apply the full vector finite element method [27] to investigate the mode loss, the birefringence of this fiber and the corresponding frequency region for single-mode THz propagation.

3. Analysis and Discussion

As shown in Fig. 1, it is seen that the major axis' direction of elliptical hole might play an important role

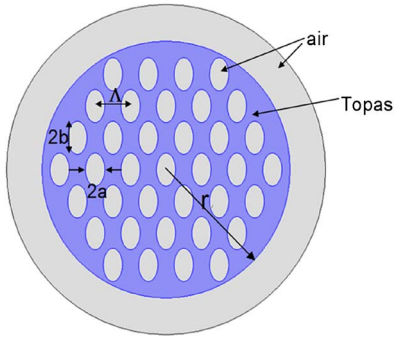

Fig. 1. Cross section of microstructure Topas fiber.

in this porous fiber since it inherently affects the geometric symmetry of the fiber. And the birefringence might be varied when one rotates the major axis. In order to check this point, let us investigate the dependence of the birefringence, $B = |n_x - n_y|$, on the rotation angle θ. Here we have defined the directions of the minor and the major axes of the air holes as the x- and y-polarization axes, respectively, and n_x and n_y are the refractive indices accordingly. Please note that $\theta = 0°$ corresponds to the case of the major-axis direction shown in Fig. 1. The simulation result is shown in Fig. 2. Note that we set the frequency at 1.1 THz as an example. It is seen from Fig. 2 that, during increasing the rotation angle θ, the birefringence increases gradually until its first maximum at $\theta = 30°$ and then decreases to the first minimum at $\theta = 60°$, and this pattern is repeated thereafter. This angle-dependent oscillatory phenomenon can be explained from the structure and layout of air holes in the fiber. When the angle is rotated to 30°, there exists the most difference of the porosity between the two orthogonal polarization directions, which will lead to the maximal birefringence. It should be pointed out that, when being rotated to 60°, the geometric configuration of the fiber is just the same as that without being rotated. This is owing to the six-fold symmetry of the hexagonal porous fiber. Therefore, the curve repeats itself three times when rotating the major axis of the elliptical hole from 0° to 180°.

Let us take the rotation angle of 15°, 30°, and 45° as examples to investigate the dependence of the birefringence on the frequency. The corresponding cross sections of the fibers are shown in Figs. 3(a)–3(c) and the simulation result is shown in Fig. 3(d). Note that the result for the nonrotation case ($\theta = 0°$) is also plotted in Fig. 3(d) for comparison. It is seen that rotating the major axis of the elliptical hole can significantly influence the birefringence. Indeed, owing to the identical symmetry relative to the case for $\theta = 30°$, the birefringence under the rotation angle of 15° is quite close to that of 45°. To clearly see this point, a small segment of the curves for 15° and 45° is also plotted in Fig. 3(d) (see the inset).

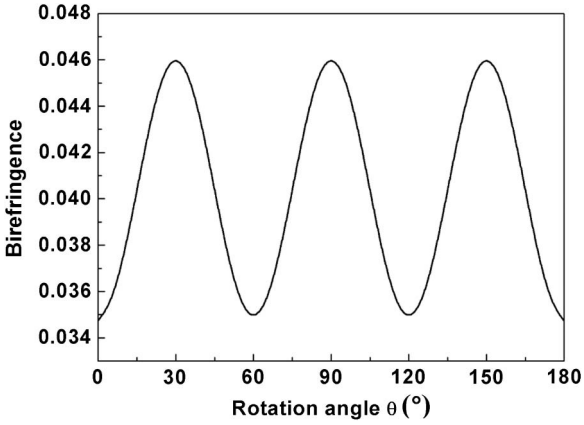

Fig. 2. Birefringence versus different rotation angles.

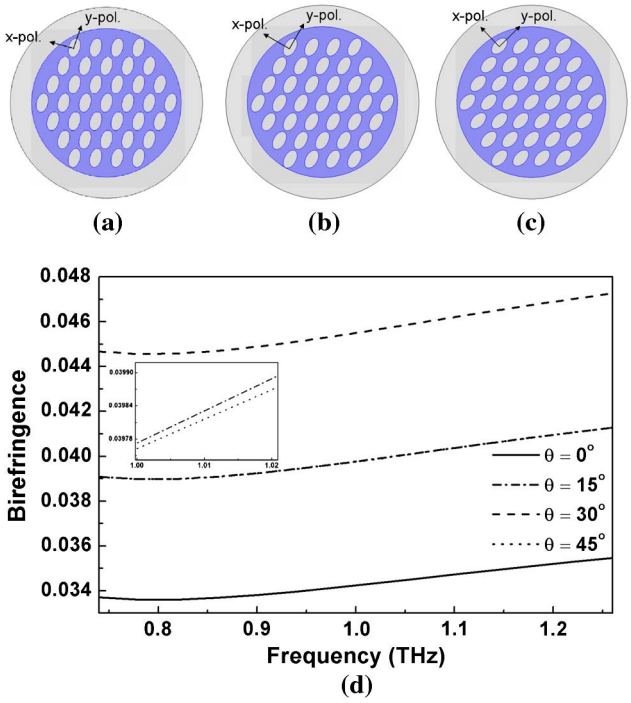

Fig. 3. (a)–(c) are the cross sections of microstructure Topas fibers. Clockwise rotate the elliptical holes' major axis by (a) 15°, (b) 30°, and (c) 45°. (d) is the birefringence as a function of the frequency for different rotating angles in the condition of single mode. The solid line indicates the birefringence without rotating; the dashed–dotted line, dashed line, and dotted line indicate the birefringence corresponding to (a), (b), and (c), respectively. Inset: magnified birefringence segment for the rotation angles of 15° and 45°.

In addition, we take several frequencies as examples to see whether such rotating would influence the single-mode property or not. It is well known that in a birefringent fiber the refractive indices in two orthogonal polarization directions are different. In our porous fiber, the porosity along the y axis is always larger than that along the x axis, meaning that the n_{eff} and thus the V-parameter of the y-polarization mode are smaller than that of the x-polarization mode. Therefore, for completely guaranteeing that both the x- and y-polarization modes are single polarization modes, we should select the larger V-parameter, i.e., the V-parameter in the x-polarization mode. Table 1 shows the V-parameters of the x-polarization mode under the rotating angles of 0°, 15°, 30°, and 45°. The frequency is selected from 1.10 to 1.26 THz, with a step of 0.04 THz. It is seen from Table 1 that rotating to different angles just

Table 1. *V*-Parameter of Different Rotation Angles at Different Frequencies

Frequency (THz)	$V_{\text{rotate0°}}$	$V_{\text{rotate15°}}$	$V_{\text{rotate30°}}$	$V_{\text{rotate45°}}$
1.10	2.00	2.01	2.02	2.01
1.14	2.12	2.13	2.15	2.13
1.18	2.23	2.25	2.26	2.25
1.22	2.35	2.37	2.38	2.37
1.26	2.47	2.49	2.50	2.48

arises little change in the V-parameter. This means that it provides us a good benefit to enhance the birefringence while not worrying about decreasing the single-mode propagation bandwidth. Also, please note that this is simply realized by only rotating the major axis of air hole.

Based on the discussion above, in the following simulations we focus on the fiber with the rotation angle of 30°. First, let us investigate the dependences of the n_{eff}, the V-parameter, and the birefringence on the frequency. The corresponding results are shown in Figs. 4(a)–4(c), respectively. It is seen from Fig. 4(a) that the n_{eff} of the y-polarization mode drops under 1 at the frequency of 0.73 THz, thus leading to a long-wavelength cutoff for wave guidance. On the other hand, it is seen from Fig. 4(b) for the V-parameter that the single-mode cutoff frequency is approximately 1.22 THz. After knowing these two points, we calculate the birefringence of the fiber, as shown in Fig. 4(c), in the frequency range from 0.73 to 1.22 THz. Note that in such a frequency range the fiber guides only the fundamental mode and at the same time the high birefringence is obtained. The birefringence as high as ~0.047 is obtained at 1.22 THz, which is much higher compared with Ref. [18] where the birefringence is 0.03 for the same ρ and the same frequency.

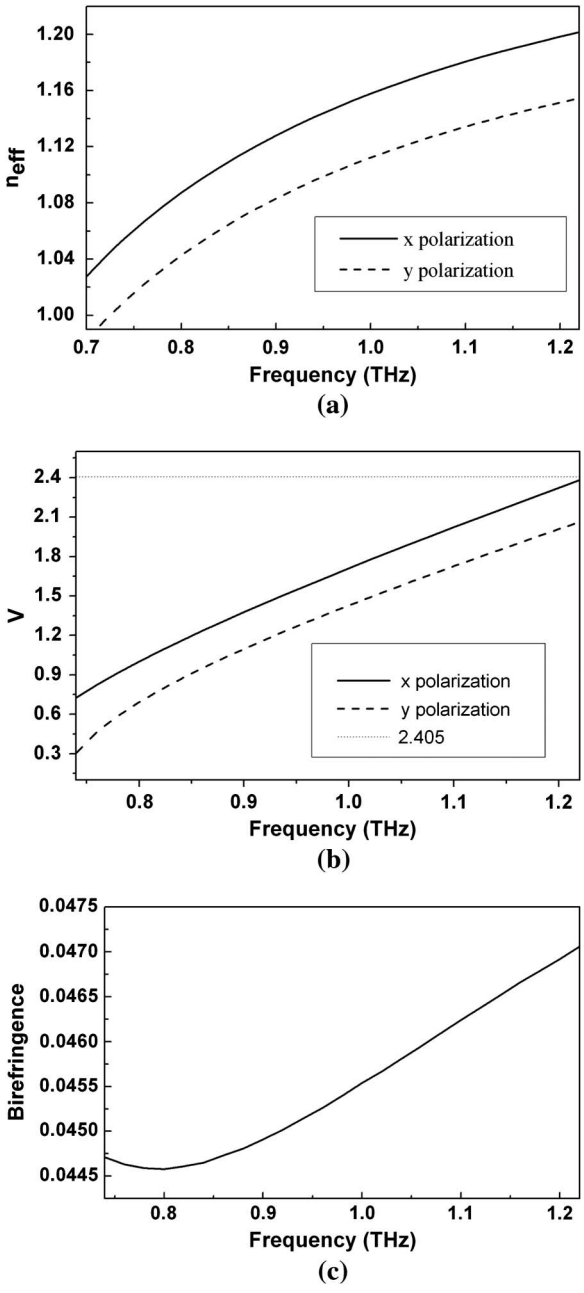

Fig. 4. (a) n_{eff}, (b) the V-parameter, and (c) the birefringence properties of the fiber proposed in Fig. 3(b) versus the frequency.

Second, let us discuss the loss property of this kind of fiber. The major loss mechanism of this porous microstructure fiber is the material absorption. For a given mode, the material absorption loss usually causes effective mode loss, defined by [28]

$$\alpha_{\text{mod}} = \frac{(\varepsilon_0/\mu_0)^{1/2} n \alpha_{\text{mat}} \int_{\text{material}} |\mathbf{E}|^2 \mathrm{d}A}{\mathrm{Re}\left\{\hat{z} \cdot \int_{\text{all}} \mathbf{E} \times \mathbf{H}^* \mathrm{d}A\right\}}, \qquad (2)$$

where ε_0 and μ_0 are the permittivity and the permeability in vacuum, respectively. n is the refractive index of the material and α_{mat} is the absorption loss of the bulk material. $\mathbf{E}$ is the electric field component, $\mathbf{H}^*$ is the complex conjugated magnetic field component and $\hat{z}$ is the unit vector in the z direction. The word "all" means that the integral covers the entire regions of the air holes, Topas, and air cladding. As for Topas, α_{mat} is linearly proportional to the frequency in the range from 0.2 to 1.6 THz, and it is 0.06 cm^{-1} at 0.4 THz and increases at a rate of 0.36 cm^{-1}/THz [25]. For the same single mode range from 0.73 to 1.22 THz, we calculate the dependences of the α_{mod}s of the two polarized modes on the frequency and plot the result in Fig. 5(a). It is seen that α_{mod} increases as the frequency for each polarization mode. This is mainly determined by the intrinsic bulk material absorption. Moreover, the α_{mod} of the x-polarization mode is larger than that of the y-polarization mode. Please note that the n_{eff} of the former is larger, meaning that more electromagnetic fields exist in the Topas and are being dissipated gradually in it. Let us compare the loss of our fiber with other fibers for THz-wave guiding. Since the bulk material loss of Topas is much lower than that of other polymer materials, it is easy to think that a lower loss can be obtained in such a Topas-based porous fiber we designed. This is really a fact if one consults the Teflon-based porous fiber [18] and the PMMA-based one [24]. In addition, it is seen from Fig. 5(a) that the y-polarization mode has the mode loss lower than 0.1 dB/cm at the frequency around 0.8 THz, while at nearly the same frequency a loss of 0.43 dB/cm was reported in a kind of Topas-based porous fiber [25].

To further see the loss property, we introduce another parameter: the relative mode loss, which is defined by $\eta = \alpha_{\text{mod}}/\alpha_{\text{mat}}$. The relative mode loss

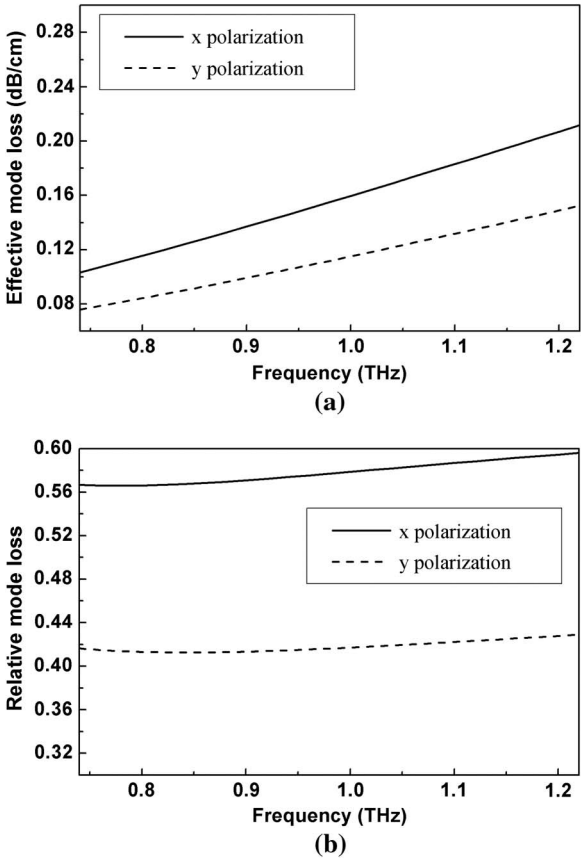

Fig. 5. (a) Effective mode loss and (b) relative mode loss versus the frequency.

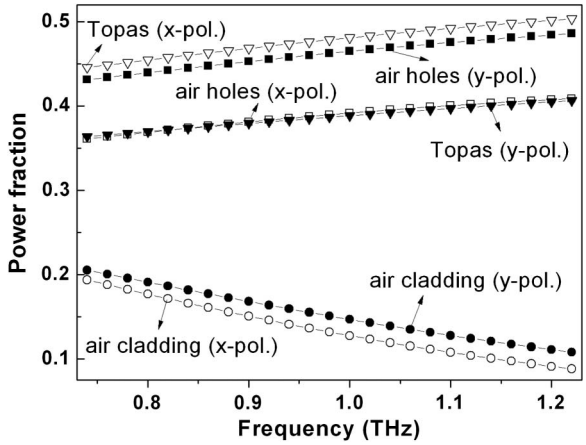

Fig. 6. Power distribution fractions of mode power guided in air holes, air cladding, and Topas for both two fundamental orthogonal polarization modes.

property as a function of the frequency is shown in Fig. 5(b). It can be seen that the ηs of x- and y-polarization modes are around 0.55 and 0.4, respectively. Therefore, the loss of y-polarization mode is decreased to only 40% compared with the bulk material absorption, which is quite acceptable.

Finally, we quantify the fraction of mode power propagating in the air (including the air holes and the air cladding) and in the Topas as a function of frequency. Such an investigation might give the details of the energy distribution in the fiber, thus is helpful for us to further design a low-loss fiber. Let us define the Poynting vector along the propagation direction as S_z, the fraction of mode power η' can be expressed by

$$\eta' = \frac{\int_X S_z \mathrm{d}A}{\int_{\mathrm{all}} S_z \mathrm{d}A}, \tag{3}$$

where X represents the integral region which one interests. In our simulation, we choose X as the entire air holes, the Topas material and the air cladding, respectively. The corresponding η's as functions of frequencies are shown in Fig. 6. It is seen that most of the mode power are confined in air holes and Topas. It is also easily seen that a higher power fraction in Topas along the x axis leads to a higher loss, which is exactly coincident with the discussion above. Besides, among the three parts of the light energy, only less than 20% of the power fraction is transported outside the fiber core. And as the frequency increases, power fraction in the air cladding monotonically decreases. The power flow distributions of the x- and y-polarization fundamental modes at 1 THz are shown in Figs. 7(a) and 7(b), respectively. It indicates that the mode power is well confined in the fiber core.

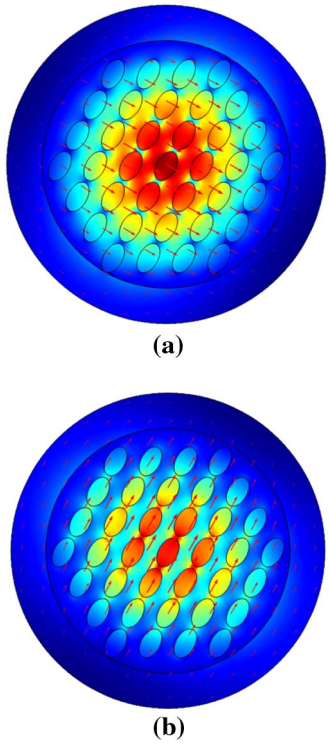

Fig. 7. (a) and (b) indicate the power flow distributions of the x- and y-polarization fundamental modes at 1 THz, respectively.

4. Conclusions

A kind of highly birefringent polymer porous fiber with low-loss property is proposed in this paper. It is found that, to guarantee the single mode condition at the THz frequency range, the fiber's radius should be restrained; the birefringence can be enhanced by rotating the major axis of the elliptical air-hole and there exists an optimal rotating angle at 30°. A birefringence of ~0.047 can be obtained at the ellipticity of 0.6 under the optimal rotating angle; the effective mode loss in the single mode range from 0.73 to 1.22 THz can be well suppressed no larger than 0.21 and 0.15 dB/cm, respectively for the x- and the y-polarization modes.

This work was supported in part by the West Light Foundation of the Chinese Academy of Sciences (CAS) under Grant 2009LH01, the National Natural Science Foundation of China under Grants 60778020 and 61275149, the Innovation Foundation of CAS under Grant CXJJ-11-M22, and the Advanced Programs of Technological Activities for Overseas Scholars.

References

1. R. H. Jacobsen, D. M. Mittleman, and M. C. Nuss, "Chemical recognition of gases and gas mixtures with terahertz waves," Opt. Lett. **21**, 2011–2013 (1996).
2. Q. Chen, Z. P. Jiang, G. X. Xu, and X. C. Zhang, "Near-field terahertz imaging with a dynamic aperture," Opt. Lett. **25**, 1122–1124 (2000).
3. Y. F. He, P. I. Ku, J. R. Knab, J. Y. Chen, and A. G. Markelz, "Protein dynamical transition does not require protein structure," Phys. Rev. Lett. **101**, 178103 (2008).
4. N. Laman, S. S. Harsha, D. Grischkowsky, and J. S. Melinger, "7 GHz resolution waveguide THz spectroscopy of explosives related solids showing new features," Opt. Express **16**, 4094–4105 (2008).
5. L. Ho, M. Pepper, and P. Taday, "Terahertz spectroscopy: signatures and fingerprints," Nat. Photonics **2**, 541–543 (2008).
6. J. Q. Zhang and D. Grischkowsky, "Waveguide terahertz time-domain spectroscopy of nanometer water layers," Opt. Lett. **29**, 1617–1619 (2004).
7. K. Wang and D. M. Mittleman, "Metal wires for terahertz wave guiding," Nature **432**, 376–379 (2004).
8. T. I. Jeon, J. Q. Zhang, and D. Grischkowsky, "THz Sommerfeld wave propagation on a single metal wire," Appl. Phys. Lett. **86**, 161904 (2005).
9. J. A. Harrington, R. George, and P. Pedersen, "Hollow polycarbonate waveguides with inner Cu coatings for delivery of terahertz radiation," Opt. Express **12**, 5263–5268 (2004).
10. B. Bowden, J. A. Harrington, and O. Mitrofanov, "Silver/polystyrene-coated hollow glass waveguides for the transmission of terahertz radiation," Opt. Lett. **32**, 2945–2947 (2007).
11. A. Hassani, A. Dupuis, and M. Skorobogatiy, "Low loss porous terahertz fibers containing multiple subwavelength holes," Appl. Phys. Lett. **92**, 071101 (2008).
12. A. Hassani, A. Dupuis, and M. Skorobogatiy, "Porous polymer fibers for low-loss terahertz guiding," Opt. Express **16**, 6340–6351 (2008).
13. M. Skorobogatiy and A. Dupuis, "Ferroelectric all-polymer hollow Bragg fibers for terahertz guidance," Appl. Phys. Lett. **90**, 113514 (2007).
14. K. Nielsen, H. K. Rasmussen, P. U. Jepsen, and O. Bang, "Porous-core honeycomb bandgap THz fiber," Opt. Lett. **36**, 666–668 (2011).
15. J. Liang, L. Y. Ren, N. N. Chen, and C. H. Zhou, "Broadband, low-loss, dispersion flattened porous-core photonic bandgap fiber for terahertz (THz)-wave propagation," Opt. Commun. **295**, 257–261 (2013).
16. H. L. Bao, K. Nielsen, H. K. Rasmussen, P. U. Jepsen, and O. Bang, "Fabrication and characterization of porous-core honeycomb bandgap THz fibers," Opt. Express **20**, 29507–29517 (2012).
17. S. Atakaramians, S. A. Vahid, B. M. Fischer, D. Abbott, and T. M. Monro, "Porous fibers: a novel approach for low loss THz waveguides," Opt. Express **16**, 8845–8854 (2008).
18. H. B. Chen, D. R. Chen, and Z. Hong, "Squeezed lattice elliptical-hole terahertz fiber with high birefringence," Appl. Opt. **48**, 3943–3947 (2009).
19. L. Jing and J. Q. Yao, "Single mode condition and power fraction of air-cladding of total refractive guided porous polymer terahertz fibers," Chin. Phys. Lett. **28**, 084202 (2011).
20. X. G. Jiang, D. R. Chen, and G. F. Hu, "Suspended hollow core fiber for terahertz wave guiding," Appl. Opt. **52**, 770–774 (2013).
21. S. E. Kim, B. H. Kim, C. G. Lee, S. Lee, K. Oh, and C. S. Kee, "Elliptical defected core photonic crystal fiber with high birefringence and negative flattened dispersion," Opt. Express **20**, 1385–1391 (2012).
22. D. R. Chen and L. F. Shen, "Highly birefringent elliptical-hole photonic crystal fibers with double defects," J. Lightwave Technol. **25**, 2700–2705 (2007).
23. Y. Yue, G. Y. Kai, T. T. Sun, Z. Wang, L. Jin, Y. F. Lu, C. S. Zhang, J. G. Liu, Y. Li, Y. G. Liu, S. Z. Yuan, and X. Y. Dong, "Highly birefringent elliptical-hole photonic crystal fiber with squeezed hexagonal lattice," Opt. Lett. **32**, 469–471 (2007).
24. S. Atakaramians, S. A. Vahid, H. E. Heidepriem, M. Nagel, B. M. Fischer, D. Abbott, and T. M. Monro, "THz porous fibers: design, fabrication and experimental characterization," Opt. Express **17**, 14053–14062 (2009).
25. S. Atakaramians, S. A. Vahid, B. M. Fisher, D. Abbott, and T. M. Monro, "Low loss, low dispersion and highly birefringent terahertz porous fibers," Opt. Commun. **282**, 36–38 (2009).
26. K. Nielsen, H. K. Rasmussen, A. J. L. Adam, P. C. M. Planken, O. Bang, and P. U. Jepsen, "Bendable, low-loss Topas fibers for the terahertz frequency range," Opt. Express **17**, 8592–8601 (2009).
27. K. Saitoh and M. Koshiba, "Single-polarization single-mode photonic crystal fibers," IEEE Photon. Technol. Lett. **15**, 1384–1386 (2003).
28. B. Ung, A. Mazhorova, A. Dupuis, M. Rozé, and M. Skorobogatiy, "Polymer microstructured optical fibers for terahertz wave guiding," Opt. Express **19**, B848–B861 (2011).